How well do we know the seasonal cycle in ocean bottom pressure?

R. M. Ponte[1], M. Zhao[1], and M. Schindelegger[2]

[1]Atmospheric and Environmental Research, Inc., Lexington, Massachusetts, USA
[2]Institute of Geodesy and Geoinformation, University of Bonn, Germany

Key Points:

- Substantial differences remain in satellite and model-based estimates of the mean seasonal cycle in ocean bottom pressure (p_b)
- Differences between two satellite gravimetry products suggest largest uncertainties around many continental boundaries
- Absence of gravitational attraction and loading effects and intrinsic ocean variability can lead to errors in model-based p_b estimates

Corresponding author: R. M. Ponte, rponte@aer.com

Abstract

We revisit the nature of the ocean bottom pressure (p_b) seasonal cycle by leveraging the mounting GRACE-based p_b record and its assimilation in the ocean state estimates produced by the project for Estimating the Circulation and Climate of the Ocean (ECCO). We focus on the mean seasonal cycle from both data and ECCO estimates, examining their similarities and differences and exploring the underlying causes. Despite substantial year-to-year variability, the 21-year period studied (2002–2022) provides a relatively robust estimate of the mean seasonal cycle. Results indicate that the p_b annual harmonic tends to dominate but the semi-annual harmonic can also be important (e.g., subpolar North Pacific, Bellingshausen Basin). Amplitudes and short-scale phase variability are enhanced near coasts and continental shelves, emphasizing the importance of bottom topography in shaping the seasonal cycle in p_b. Comparisons of GRACE and ECCO estimates indicate good qualitative agreement, but considerable quantitative differences remain in many areas. The GRACE amplitudes tend to be higher than those of ECCO typically by 10%–50%, and by more than 50% in extensive regions, particularly around continental boundaries. Phase differences of more than 1 (0.5) months for the annual (semiannual) harmonics are also apparent. Larger differences near coastal regions can be related to enhanced GRACE data uncertainties and also to the absence of gravitational attraction and loading effects in ECCO. Improvements in both data and model-based estimates are still needed to narrow present uncertainties in p_b estimates.

Plain Language Summary

We revisit the nature of the ocean bottom pressure (p_b) seasonal cycle by leveraging the mounting data from space gravity missions and their use in constraining model-based estimates produced by the project for Estimating the Circulation and Climate of the Ocean (ECCO). We focus on the mean seasonal cycle from both data and ECCO estimates, examining their similarities and differences and exploring the underlying causes. Despite substantial year-to-year variability, the 21-year period studied (2002–2022) provides a relatively robust estimate of the mean seasonal cycle. The p_b annual cycle tends to dominate but the semi-annual cycle can also be important in some regions. Amplitudes are enhanced near shallow coastal regions and can also vary more strongly across the coastal zone, pointing to the importance of changes in ocean bottom topography in shaping the seasonal cycle in p_b. Comparisons of data and ECCO estimates indicate good qualitative agreement, but considerable quantitative differences in the magnitude and timing of maxima remain. Largest differences, which tend to occur near coastal regions, can be related to enhanced data uncertainties and also to the absence in ECCO of effects from gravitational attraction of land ice and water storage and related deformation of the ocean bottom.

1 Introduction

Pressure is a fundamental variable for describing the dynamics of geophysical fluids and is strongly related to kinematics through the geostrophic relation. Knowledge of the 3-dimensional pressure field in the oceans can portray in detail the dominant circulation: its inference based on only temperature and salinity (density) fields was for a long time a main challenge in oceanography (e.g., Wunsch, 1996). With the advent of satellite altimetry came the ability to determine surface pressure and thus absolute pressure over the full water column, provided sufficient coverage of density measurements. The latter has been proving difficult to realize though, with the Argo program still mostly confined to the upper 2000 m.

In this context, knowledge of ocean bottom pressure (p_b) can add important information about the deep pressure fields and related circulation. However, measurements of p_b on a global scale and continuously in time only became possible with the launch of GRACE in 2002 (Tapley et al., 2004) and more recently its follow-on mission (Landerer et al., 2020).

Prior to the space gravimetry era, very little was known about variable p_b over the global ocean. The main studies on global characteristics of p_b variability (Gill & Niller, 1973; Ponte, 1999), separated by almost 3 decades, focused on the seasonal cycle and were based on simple vorticity and Ekman dynamics (Gill & Niller, 1973) and a global ocean general circulation model (Ponte, 1999). Fully testing the model-based estimates in Gill and Niller (1973) and Ponte (1999) was, however, not possible due to the lack of appropriate observations.

More than 20 years after the onset of space gravity measurements, much has been learned about p_b variability and in particular about its seasonal cycle using both GRACE data and models (Kanzow et al., 2005; Bingham & Hughes, 2006; Ponte et al., 2007; Vinogradov et al., 2008; Peralta-Ferriz & Morison, 2010; Johnson & Chambers, 2013; Piecuch & Ponte, 2014; Piecuch, 2015; Cheng et al., 2021; Xiong et al., 2022; Chen et al., 2023). Early, relatively noisy estimates of the seasonal cycle based on the initial releases of the GRACE data (Kanzow et al., 2005; Bingham & Hughes, 2006; Ponte et al., 2007) have given way to more stable estimates based on longer records and improved data releases (Johnson & Chambers, 2013; Cheng et al., 2021). Although observations and simplified models consistently represent major features of the seasonal cycle in p_b and provide a similar qualitative description of its properties at regional scales (e.g., Peralta-Ferriz & Morison, 2010; Piecuch & Ponte, 2014; Piecuch, 2015), it is also evident that substantial differences remain in seasonal behavior when examined over the global oceans (e.g., Cheng et al., 2021; Xiong et al., 2022).

In the present work, we take advantage of the mounting space-based p_b record, and its assimilation in the model-based estimates produced by the project for Estimating the Circulation and Climate of the Ocean (ECCO; Wunsch et al., 2009), to revisit the nature of the p_b seasonal cycle from a global perspective. We are particularly interested in defining the mean seasonal cycle from both data and ECCO, examining in detail their similarities and differences, and exploring their underlying causes. As one of the main climate signals in p_b (see Figure 3 in Ponte, 1999), the seasonal cycle provides an excellent basis to assess both data and model strengths and shortcomings. Our analyses also aim to provide estimates of the mean p_b seasonal cycle along with a measure of uncertainty that can serve as a reference for future studies.

In the remainder of this paper, we describe the GRACE data and ECCO fields along with pertinent methods of analysis (Section 2), examine the general characteristics of the various mean seasonal cycle estimates (Section 3), explore their year-to-year variability (Section 4), and compare data and ECCO results to assess uncertainties and their causes (Section 5). A final section provides a general discussion and summary of our findings. Throughout the work, we label the annual oscillation in p_b and its first and second harmonics as Sa, Ssa, and Sta, conforming with the nomenclature used by Ray et al. (2021) for the seasonality in sea level.

2 Data, Models and Methodology

2.1 GRACE Fields

We use monthly p_b mascon solutions from GRACE and GRACE-FO gravity field inversions by two centers: Jet Propulsion Laboratory (JPL, RL06.1M.MSCNv03, Watkins et al., 2015; Wiese et al., 2023) and Goddard Space Flight Center (GSFC, RL06v2.0_OBP, Loomis et al., 2019). The particular version of the JPL product covers the time period from April 2002 to November 2022, with p_b data discretized in the form of $3^\circ \times 3^\circ$ equal-area caps. The GSFC mascons, available from April 2002 to December 2022 at this writing, are provided on an equal-angle $1/2^\circ$ grid. Data in some months are unavailable due to issues like instrument problems, calibration campaigns, and gap between the two missions. For both datasets, monthly global mean values are subtracted to remove p_b signals associated with the inverted barometer effect and the net freshwater transfer into the ocean from land and

atmosphere. In addition, we apply an *ad hoc* correction for the bottom pressure signatures of four major earthquake events (2007 Sumatra-Andaman, 2010 Maule, 2011 Tohoku-Oki, 2012 Indian Ocean; Han et al., 2013). For each of these events, we define a ∼5–10° area around the source location, discard at every grid point the two monthly p_b values at and immediately after the earthquake, and detrend (separately) the remaining time series segments.

2.2 ECCO Output

The ECCO project provides global ocean state estimates, comprising important variables such as p_b, by constraining the Massachusetts Institute of Technology general circulation model to most available ocean observations in a weighted-least-squares optimization procedure (e.g., Wunsch et al., 2009; Forget et al., 2015; Fukumori et al., 2019). Minimization of the overall model-data misfits is achieved by adjusting atmospheric boundary conditions, internal model parameters, and initial conditions, within estimated uncertainties. Given that ECCO solutions are constrained by other observations beyond GRACE and GRACE-FO data, they represent a comprehensive synthesis of information from all available data. Comparisons of ECCO and GRACE provide a measure of uncertainty in the respective p_b estimates, stemming from both data and model issues.

In this study, we use p_b output from the latest ECCO product (version 4 release 5 or v4r5 hereafter). The horizontal resolution varies from 22 km in low and high latitudes to 111 km (nominal $1^\circ \times 1^\circ$) in mid latitudes (O. Wang et al., 2020). Monthly p_b fields are available between January 1992 and June 2023. Note that after 2019, ECCOv4r5 is not constrained to observations. We did not find noticeable differences in the seasonal cycle characteristics when including the latter period without observational constraints. Global-mean values of p_b are removed in each month, given our focus on dynamically relevant p_b signals. As with the GRACE data, we take p_b as pressure value normalized by ρg, where $\rho = 1030$ kg m^{-3} is sea water density and $g = 9.81$ m s^{-2} is the acceleration of gravity. In text and figures, p_b values are thus given in units of length or equivalent water thickness.

2.3 Analysis Methods

We extract the seasonal cycle and its formal standard errors from the monthly ECCO and GRACE fields using least-squares harmonic analysis at each grid point. To minimize inter-product discrepancies brought on by different resolutions and sampling months, we first average p_b fields from GSFC mascons and ECCO to match the grids in JPL mascons, and then apply the harmonic analysis over common months across both GRACE products and ECCO estimates. Our phase convention is as in Ray et al. (2021) and all three harmonics (Sa, Ssa, Sta) are considered in the fit. These oscillations are written as $A\cos[\Theta(t) - G]$, where A is amplitude, G is phase lag, and the argument $\Theta(t)$ is taken relative to the vernal equinox, thus tying the seasonality to its main physical cause. For the annual cycle, $\Theta(t)$ equals h, the sun's mean ecliptic longitude with periodicity of a tropical year (Doodson, 1928; Ray et al., 2021). Arguments for semiannual and terannual terms are defined accordingly, that is, $\Theta(t) = 2h$ (Ssa) and $\Theta(t) = 3h$ (Sta).

To assess the representativeness of the mean seasonality derived from 21 years, we calculate standard deviations and standard errors from the 21 yearly harmonics relative to their mean values. For all three frequencies under analysis, we first deduce the mean harmonics as $\sum_{n=1}^{N} A_n e^{\mathrm{i}\Theta_n}/N$, where A_n and Θ_n represent Sa, Ssa or Sta amplitude and phase in year n, and $N = 21$ is the total number of years ($\mathrm{i} \equiv \sqrt{-1}$). The resulting mean amplitude and phase values, denoted as $\overline{A}$ and $\overline{\Theta}$, are then used to calculate the standard deviation in amplitude and phase following $\sqrt{\sum_{n=1}^{N}(A_n - \overline{A})^2/N}$ and $\sqrt{\sum_{n=1}^{N}(\Theta_n - \overline{\Theta})^2/N}$. For any given year, when $|\Theta_n - \overline{\Theta}| > \pi$, this value is converted to $2\pi - |\Theta_n - \overline{\Theta}|$ to account for the cyclicity of phases. Standard errors are then given by standard deviation values scaled by $1/\sqrt{N}$.

3 Basic Characteristics of the Mean Seasonal Cycle

Estimates of the mean seasonal cycle in p_b based on both GRACE products are presented in parallel with those from ECCO. The discussion is centered on the qualitative characteristics of the seasonal cycle common to all the estimates, with detailed quantitative comparisons and differences between them presented in Section 5.

The mean seasonal cycle is portrayed in terms of its Sa, Ssa and Sta harmonics (Figures 1, 2 and 3 respectively) and also as four season means (DJF, MAM, JJA, SON) in Figure 4. In the context of the standard errors defined in Section 2 and shown in Figures 5–7, the Sa harmonic is the most well determined. Nevertheless, both Ssa and Sta harmonics exhibit amplitudes above standard errors over extensive areas of the ocean (Figures 1–3). All harmonics are thus treated in what follows.

Annual variations in p_b (Figure 1) are the largest in general. Typical Sa amplitudes of 0.5–2.5 cm are seen in most of the deep oceans, reaching a maximum $\sim$ 4 cm in the Australian-Antarctic basin. Amplitudes are substantially larger in many enclosed seas and coastal regions, up to $\sim$ 20 cm in the Gulf of Carpentaria and the Gulf of Thailand. The annual cycle tends to be weaker in the Atlantic basin relative to the Pacific and Indian Oceans, and with the (possible) exception of the subtropical South Pacific and subpolar North Pacific, there is no clear pattern of western intensification.

The larger annual cycle is also reflected in the p_b seasonal means (Figure 4). In most of the ocean, the seasonal cycle reaches its maximum in local winter and minimum in local summer. For example, in the subtropical North Pacific, the annual cycle is maximum in January, consistent with largest positive p_b anomalies in DJF and negative anomalies in JJA, with weaker anomalies in spring and fall. Regions with similar characteristics include most of the Southern Ocean, Nordic Seas, and coasts of the Barents and Kara Seas. These regions have significant annual p_b variations in response to wind-driven Ekman transports, as examined in Cheng et al. (2021). In the Beaufort Sea and the East Siberian and Laptev Seas, including their coasts in the Arctic, annual peak values occur from August to October, consistent with maximum p_b anomalies found in the fall months (Figure 4).

Away from the coasts, annual phases tend to be similar along longitude within each basin and imply no clear westward propagation. Annual phases are also somewhat similar across different basins (Figure 1). In fact, most of the Indian, Pacific (except the subtropical North Pacific) and Arctic Oceans on one hand, and the Atlantic and Southern Oceans on the other, show anomalies of the same sign in DJF and JJA seasons (Figure 4). Such behavior is consistent with previous results (e.g., Ponte, 1999; Vinogradov et al., 2008; Johnson & Chambers, 2013) and can be attributed to large-scale wind forcing patterns and the efficient adjustment of the mass field over the global ocean at the annual time scale.

In contrast to the homogeneous Sa phases over the deep ocean, sharper phase transitions can be seen near many coastal regions (e.g., along eastern North America and eastern Asia). This phase behavior suggests more complex (shorter scale) spatial structures of the annual cycle in coastal regions, where dynamical regimes are likely affected by water depth and bottom topography (e.g., Chen et al., 2023). Such coastal influences can still leave their imprint on the relatively coarse-resolution ($\sim 3°$) fields analyzed in Figures 1 and 4.

While Sa is the largest harmonic over most of the deep oceans, semiannual (Ssa) variations are non-negligible (Figure 2) and can be as or more important in some regions, such as the Bellingshausen Basin and the western subpolar North Pacific. These deep ocean regions have Ssa amplitudes > 1 cm (Figure 2), with maximum and minimum p_b anomalies being three, and not six months apart (Figure 4). Otherwise sub-centimeter Ssa amplitudes are found over most of the deep oceans.

Similar to Sa, many enclosed seas and coastal regions exhibit enhanced Ssa amplitudes (maxima > 3 cm around the Maritime Continent and in the Red Sea and also relatively

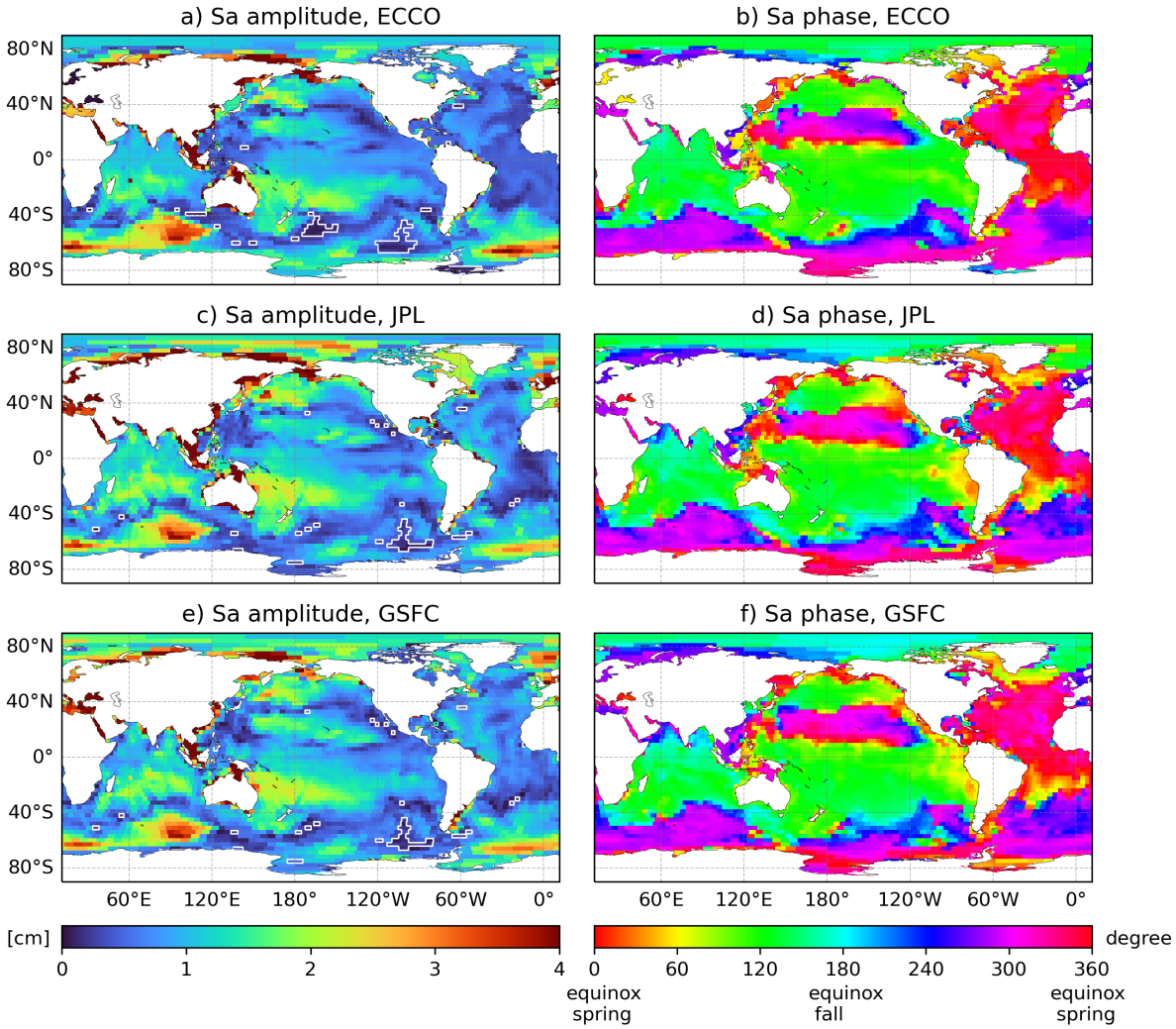

Figure 1. Annual (Sa) amplitude (cm, left) and phase (relative to the vernal equinox in degrees, right) calculated from monthly p_b record in ECCOv4r5 (a,b), JPL GRACE (c,d), and GSFC GRACE (e,f) between 2002 and 2022. White contours in the left panels denote areas where amplitudes are smaller than the standard errors.

large values along East Siberia and around the Bering Strait). Semiannual phases show, however, considerably more spatial structure than Sa phases (cf. Figures 1 and 2), not just around coastal regions but also in the deep oceans. There is also more spread in the phases from the three products, suggestive of noisier and consequently more variable estimates. We return to these differences in more detail in the next section.

The terannual component (Sta, Figure 3) is the weakest of the three harmonics and also the most uncertain when examined in terms of respective standard errors (Figures 3a,c,e and 7). Despite noticeable large-scale differences, particularly between ECCO and GRACE phases (e.g., Indo-Pacific, subpolar North Atlantic), amplitude and phase patterns are still qualitatively similar among the different products. Aside from some coastal regions, Sta amplitudes of ~ 1 cm, well above the standard error (Figure 7), occur in the western subpolar North Pacific, Beaufort Sea, and the Australian-Antarctic basin. Smaller values of $\lesssim 4$ mm are prevalent elsewhere (Figure 3). That the Sta harmonic is relatively robust in

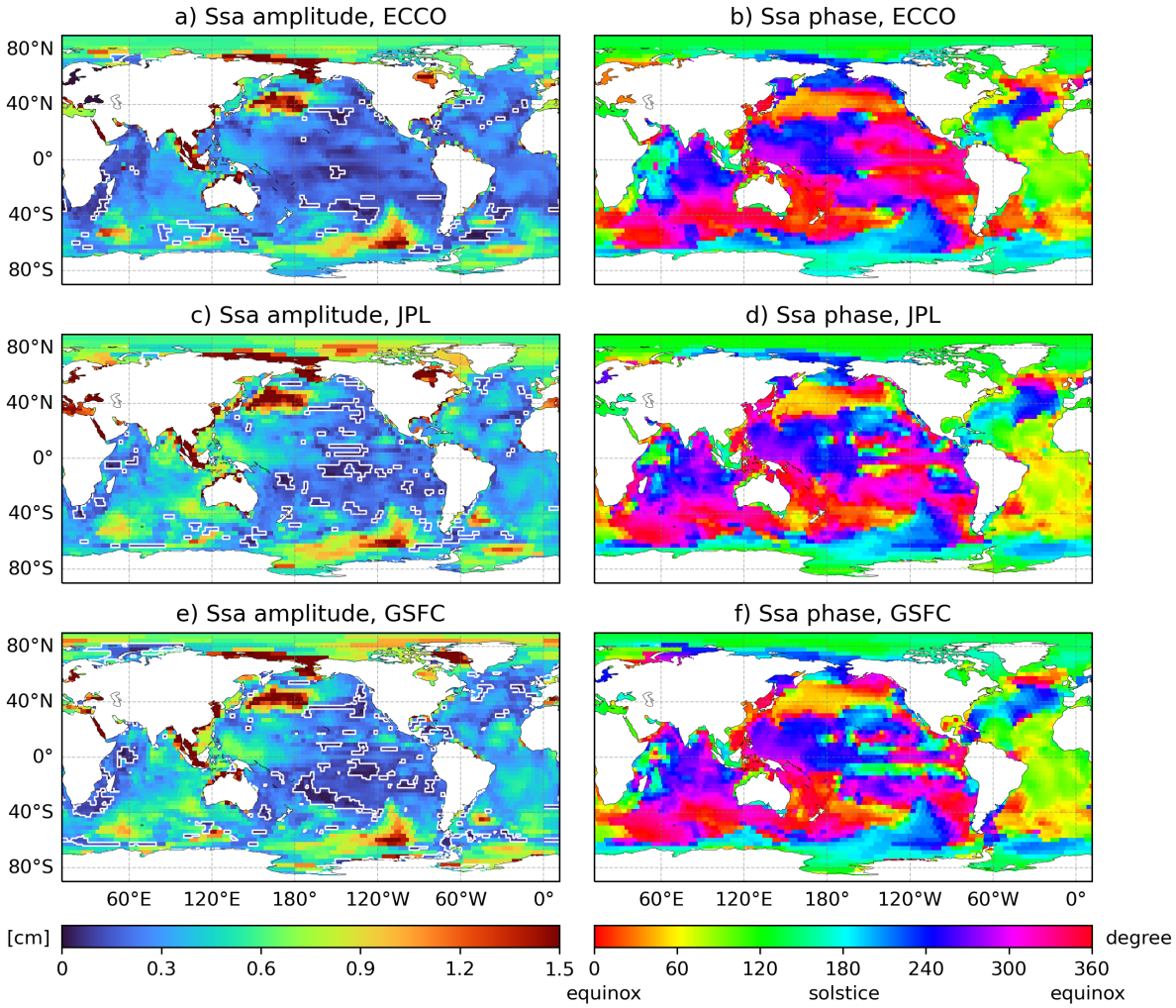

Figure 2. As in Figure 1, but for semiannual (Ssa) harmonics.

many areas despite its small values contrasts with the findings of Ray et al. (2021) for sea level. It is plausible that impacts of eddy "noise" on sea level are comparatively stronger than on p_b fields analyzed here (cf. Hughes et al., 2018). Some of this noise is also smoothed in our analysis through the use of averages over $3^\circ \times 3^\circ$ boxes.

4 Year-to-Year Variability

A general measure of overall stability of the seasonal cycle can be obtained by calculating the standard deviations of amplitude and phase over the 21 years of record (2002–2022), as described in Section 2. The resulting standard deviations in Figures 5, 6 and 7, for the Sa, Ssa and Sta harmonics, respectively, indicate substantial variations of the seasonal cycle from year to year, in comparison to the mean amplitudes and phases in Figures 1–3.

The year-to-year changes in amplitude tends to scale with the mean value, that is, largest variability coincides with places of largest mean amplitude, cf. Figures 5–7 and 1–3. This does not hold everywhere, though. For example, extensive parts of the Bellingshausen Basin show relatively variable Sa amplitudes and phases, which in turn contributes to the

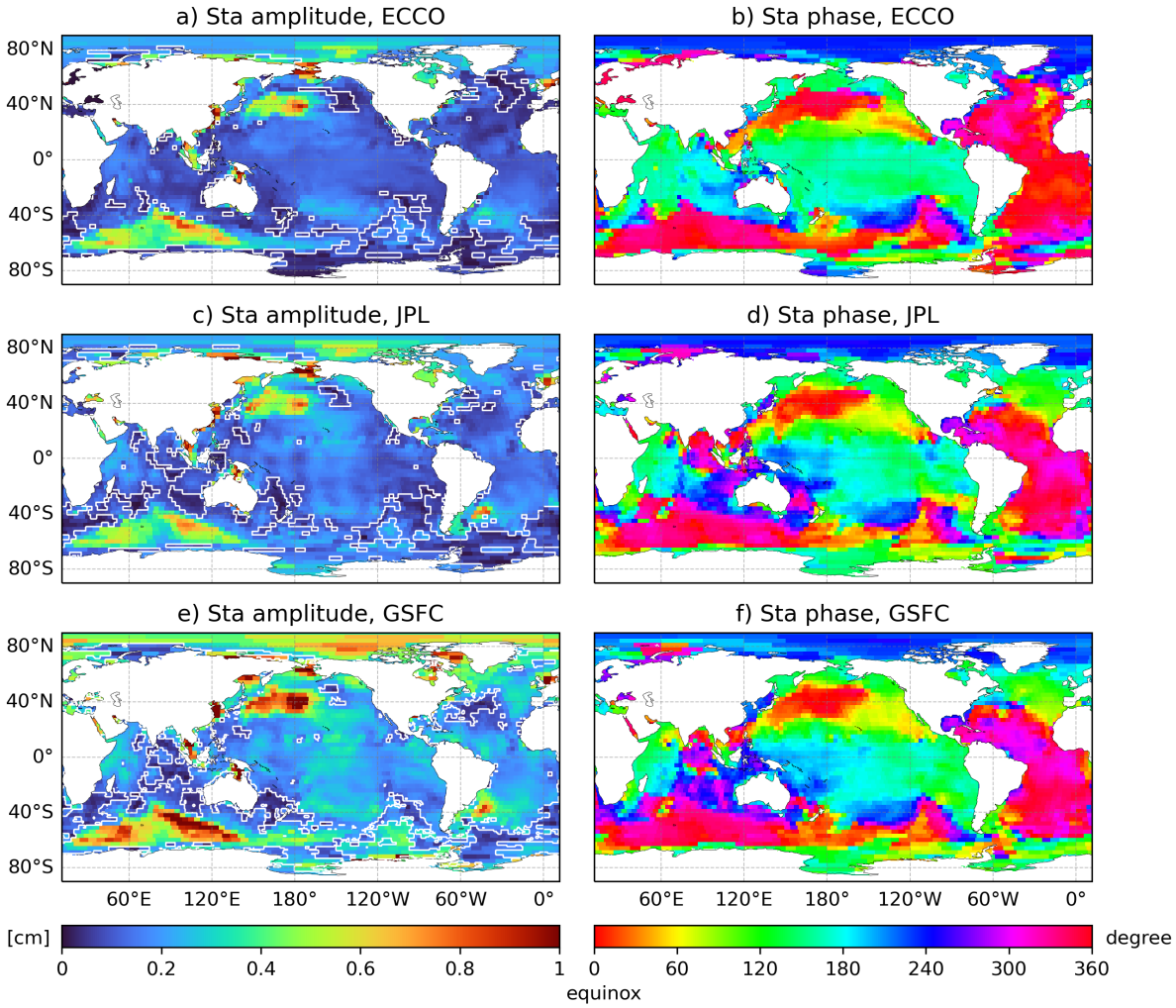

Figure 3. As in Figure 1, but for terannual (Sta) harmonics.

region's low mean amplitudes in Figure 1. Similar behavior seems to be present in the Australian-Antarctic basin for Ssa (Figures 2 and 6). In contrast, relatively stable phases can allow for a relatively strong mean seasonal cycle in some areas (e.g., Sa in the subtropical western South Pacific and Indian Oceans, Ssa in the midlatitude western North Pacific). Large (basin-scale) areas of most stable phases are found for Sa in the Indian Ocean and the western South Pacific, for both GRACE and ECCO estimates. The variability in phase tends to increase from Sa to Ssa to Sta.

Comparing results across GRACE and ECCO, there are no systematic differences in the patterns of phase variability, but higher amplitude variability is seen in GRACE for most of the global ocean and for all harmonics. Data noise and other factors, like the presence of intrinsic p_b variability in GRACE but not in ECCO (see Section5), may be partly responsible for the noted behavior.

One key question related to climate change concerns the possibility of trends in the magnitude and phasing of the seasonal cycle. Although our record length (21 years) is relatively short to address such issues, we have carried out simple linear fits of the yearly time series of amplitude for Sa, Ssa and Sta harmonics. Apart perhaps from decreasing

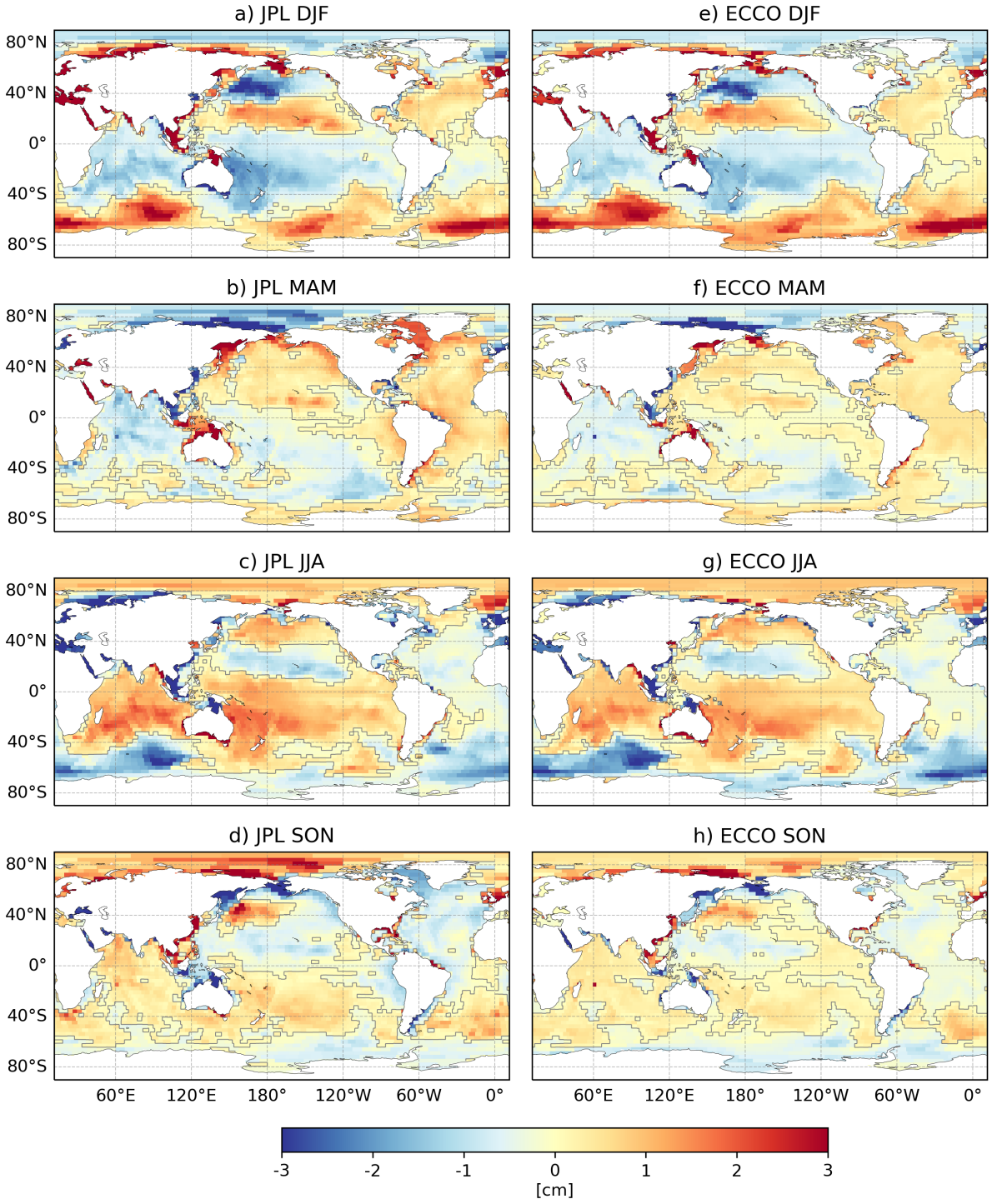

Figure 4. Mean p_b for seasons DJF (a,e), MAM (b,f), JJA (c,g) and SON (d,h), for JPL (left) and ECCOv4r5 (right). Period of analysis is 2002–2022. Seasonal anomalies based on GSFC are very similar and thus omitted to minimize clutter.

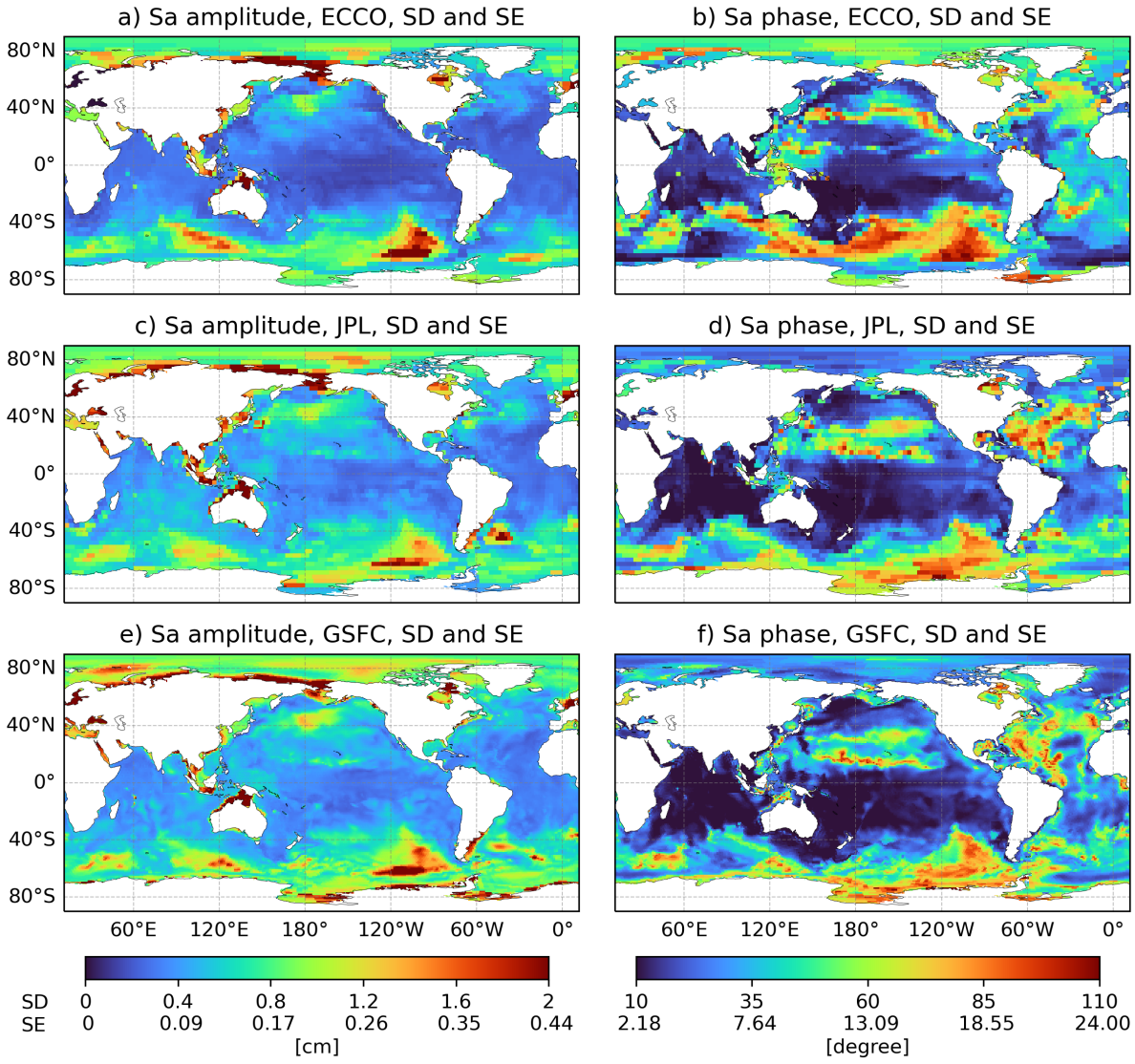

Figure 5. Annual harmonic: standard deviation (SD) of amplitude and phase for ECCO (a,b), JPL GRACE (c,d) and GSFC GRACE (e,f); colorbar ticks for standard error (SE), corresponding to SD/$\sqrt{21}$, are also provided.

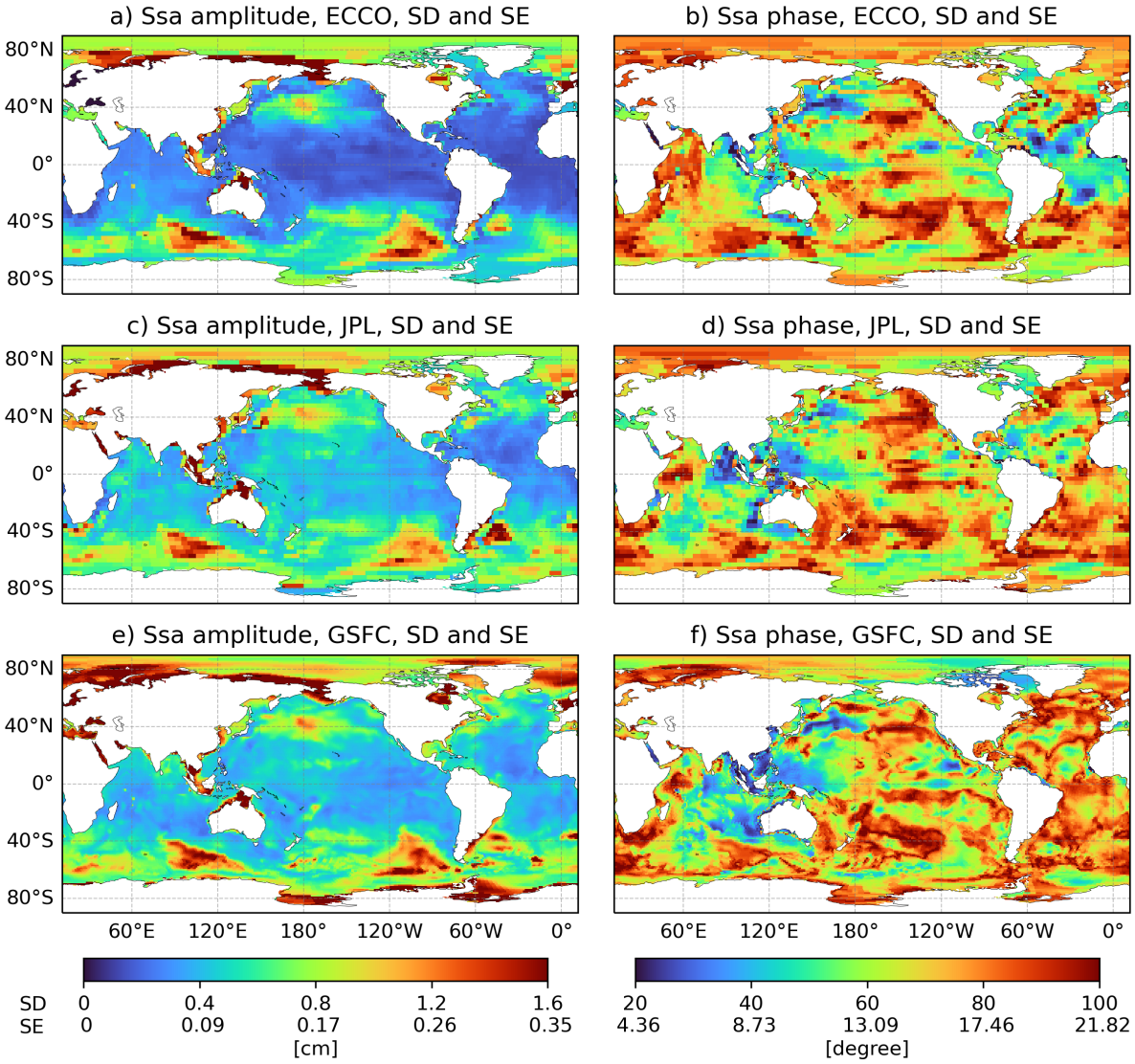

Figure 6. As in Figure 5 but for semiannual harmonic.

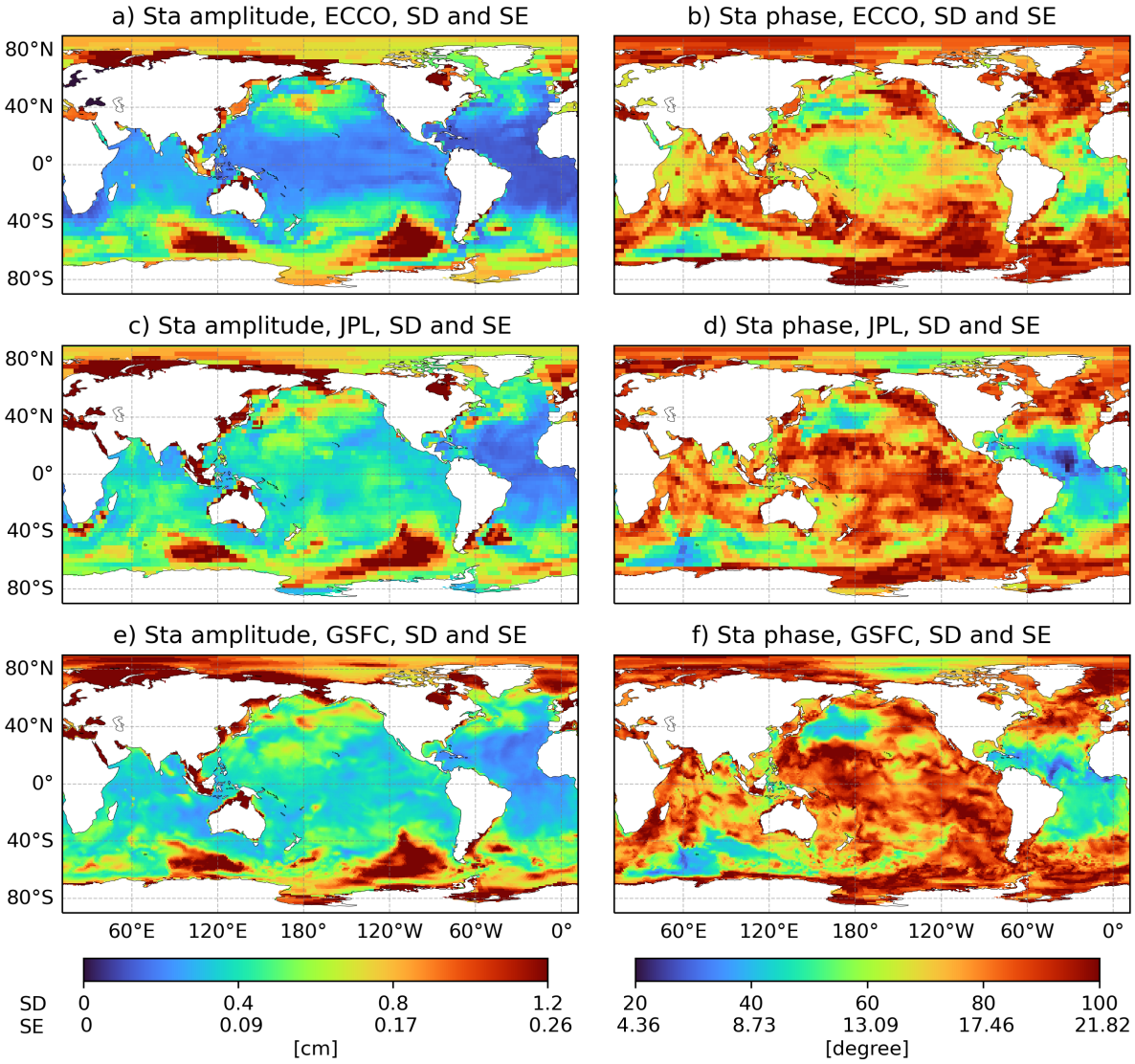

Figure 7. As in Figure 5 but for terannual harmonic.

Sa amplitudes in the East Siberian coastal regions, the results of the exploratory analysis (not shown) did not reveal any major patterns of statistically significant trends consistently present across the GRACE and ECCO products.

5 Uncertainties in the Mean Seasonal Cycle

Returning to Figures 1–4, the mean seasonal cycle in p_b estimated from GRACE data and ECCO is qualitatively similar, in terms of spatial patterns of maximum/minimum amplitudes and phases. The qualitative agreement between ECCO and GRACE is expected given that ECCO solutions are constrained by GRACE (JPL mascons), as well as by most available in situ and satellite observations. A more quantitative comparison, however, can reveal potential uncertainties in both the observations and the model-based, data-constrained ECCO estimates. We first examine differences between JPL and ECCO estimates and then elaborate on possible reasons for these differences coming from data noise and missing physics in the ocean model underlying the ECCO estimates. Focus is on the largest Sa and Ssa terms.

5.1 Assessment of JPL and ECCO Estimates

The differences between JPL and ECCO amplitudes and phases (Figure 8) imply sizable large-scale biases between the two estimates of the mean seasonal cycle. Annual amplitudes can differ by more than 0.5 cm in extensive areas, particularly around continental boundaries. Semiannual amplitude differences are generally smaller but exhibit similar enhancement near the boundaries. Differences for both harmonics amount to typically 10%–50% of their respective amplitudes, and to more than 50% in several regions (e.g., around Greenland, near South Africa, Ross Sea; Figure 8b,f). Even small percentage differences in some marginal seas with large amplitudes (e.g., Sa in the Gulf of Carpentaria or Mediterranean Sea) translate to root-mean-square (rms) differences of more than 1 cm.

The JPL GRACE amplitudes can be both larger and smaller than the ECCO amplitudes, with a tendency for larger values particularly for Sa term. The organization of these differences in large-scale patterns of the same sign suggest that uncertainties in the estimated seasonal cycles can be correlated on broad spatial scales. Salient examples in Figure 8 are the negative values for most of the Southern Ocean in the case of Sa, and the positive values for most of the Atlantic, Indian and western tropical Pacific Oceans, in the case of Ssa.

Differences in phase (Figure 8c,g) show behaviors similar to those noted for amplitudes. Sizable discrepancies of $> 30°$ (that is, > 1 or 0.5 months for Sa and Ssa, respectively) are apparent in many regions. Both positive and negative values occur on relatively large scales, with considerable portions of individual basins (e.g., Atlantic) exhibiting phase differences of mostly the same sign. As for amplitudes, there is a tendency for larger phase differences close to the continental boundaries.

The joint effect of amplitude and phase differences is captured by the rms difference also shown in Figure 8d,h. Largest values (> 1 cm) are mostly confined to coastal regions, confirming the tendency noted from the separate analysis of amplitude and phase variables. The somewhat larger rms values in Figure 8d,h compared to those in Figure 8a,e imply that both amplitude and phase differences can contribute to the estimated differences between GRACE and ECCO.

The amplitude and phase differences in Figure 8 are substantially larger than the standard errors particularly for the Sa term (Figures 5 and 6) and indicate that the year-to-year variability provide a limited view on the uncertainty of the mean p_b seasonal cycle. In other words, sampling statistics of the mean seasonal cycle cannot explain the differences between

JPL and ECCO estimates in Figure 8. Instead, the differences may rather point to either data or model (ECCO) errors, or most likely a combination of both, as explored next.

5.2 Data Uncertainties

To probe for possible data errors, we examine differences in the seasonal harmonics between the JPL and GSFC mascon products (Figure 9). Although gravity fields solutions from both sources use essentially the same sensor data (ranging, accelerometers, etc.) and can contain common errors that will be eliminated in their differences, results in Figure 9 provide an estimate of potential uncertainties resulting from different data processing, correction, and filtering techniques.

A comparison with Figure 8 reveals similar spatial patterns but for the most part with somewhat weaker magnitudes and more variability on shorter scales, for both amplitude and phase differences. A common characteristic is the tendency for larger differences to occur around the boundaries in general. There are considerable amplitude differences between JPL and GSFC fields in the Arctic and in subpolar coastal regions (e.g., around Greenland, Sea of Okhotsk), and more generally around other continental boundaries, which are similar to those in Figure 8. Largest phase differences tend to cluster also around the boundaries. Some interior ocean regions with large differences (e.g., semiannual cycle in the South Pacific) coincide with places with weak amplitudes, where more unstable phase estimates are expected.

Enhanced discrepancies in amplitude and phase estimates near the boundaries are suggestive of potential uncertainties related to the implementation of necessary filtering procedures to minimize leakage of strong seasonal variability in land ice and hydrology into oceanic p_b fields (e.g., Wiese et al., 2016). In some of these regions (e.g., around Greenland and Hudson Bay, and in the Arctic and western Mediterranean), the rms differences between JPL and GSFC can be larger than those between JPL and ECCO for both Sa and Ssa (cf. Figures 8d,h and 9d,h). Data issues are thus likely a substantial contributor to the differences with ECCO in these and other coastal regions. In a more global sense, the rms values in Figure 9 are smaller but not negligible compared to those in Figure 8 and can partly contribute to the observed mismatches between JPL and ECCO estimates of the seasonal cycle.

5.3 Model Representation Errors

A variety of factors may affect the ability of the ECCO solutions to fit the observational constraints, including those from GRACE. In particular, parts of the variability present in the satellite data may not be representable by the physics encoded in ECCO's numerical ocean model—a classic case of a representation error. One important process worth exploring here are gravitational attraction and loading (GAL) effects, especially those related to changes in land ice and terrestrial hydrology, as well as the atmosphere over land, which can cause significant seasonal p_b signals (Vinogradova et al., 2010, 2011).

These GAL effects on p_b were calculated as detailed in Appendix A, using the GSFC fields for cryospheric and hydrological mass loads and surface atmospheric pressures from an atmospheric reanalysis. The resulting Sa and Ssa variability (Figure 10), which compares well with similar estimates based on different periods and mass load datasets (e.g., Vinogradova et al., 2011), is largest around landmasses and extensive ice bodies. Most important contributions from seasonal land ice and terrestrial water storage changes occur around Eurasia, North and South America, and from the atmosphere around Eurasia (Sa) and Antarctica (Ssa). The Arctic also shows elevated GAL signals for both Sa and Ssa.

Values > 0.7 cm for Sa and > 0.2 cm for Ssa, seen near several of these continental boundaries, are appreciable when compared to Sa and Ssa p_b amplitudes in Figure 1 and 2 and are similar in magnitude to the rms differences between GRACE and ECCO (Figure

8d,h). Moreover, the larger GAL values occur in regions where there are noticeably larger rms differences between ECCO and JPL seasonal estimates (Figure 8d,h). It is therefore plausible that GAL-related variability contributes to the latter differences.

Assuming the ECCO fields do not represent any GAL variability, adding the estimated GAL effects in Figure 10 to ECCO should lead to a reduction in the mismatch to GRACE. The rms differences between ECCO and JPL data are indeed reduced in 56% (Sa) and 55% (Ssa) of the oceans when the ECCO fields are augmented with the GAL seasonal cycle (Figure 11). More importantly, largest reductions of > 5 mm (Sa) and > 2 mm (Ssa) can be seen around several landmasses, particularly in areas with largest GAL effects (e.g., around Greenland and the Amazon, near Alaska). There are clearly more larger-magnitude rms reductions than increases for both Sa and Ssa terms (Figure 11b,d). Nevertheless, basins like the Arctic show a larger mismatch between GRACE and ECCO Sa estimates when GAL effects are considered (Figure 11a). Similar results are found for Ssa in regions around Antarctica that feature relatively large atmospheric GAL effects (Figures 10f and 11c).

Several factors can cloud up the hypothesis testing in Figure 11. Given that ECCO is constrained by GRACE-derived p_b fields, it is possible that part of the GAL signals in the data are fit by the ECCO optimization, despite the absence of GAL physics in the ocean model. This could lead to double counting in our analysis. Our estimates of GAL in Figure 10 also carry the uncertainty implicit in the GSFC fields used. As another caveat, the response to GAL effects may not be fully static as assumed here, particularly in shallow and constricted regions and for the faster harmonics (see, e.g., Piecuch et al., 2022). Results in Figures 10 and 11 are nevertheless indicative that GAL effects need careful consideration in studies of the mean seasonal cycle in p_b.

Another type of representation error that can affect ECCO estimates and their difference to GRACE rests with intrinsic ocean variability, which is internally generated and not directly driven by the atmosphere (Zhao et al., 2021). Intrinsic signals are associated with nonlinear mesoscale processes and energy cascades that are not aptly modeled at the coarse resolutions used in the ECCO solution analyzed here. In particular, results in Zhao et al. (2021) indicate that such intrinsic variability has a substantial signature at the seasonal time scale.

As shown in Figure 12b, largest seasonal intrinsic variability can amount to > 0.5 cm (standard deviation) in some areas. These signals are again appreciable compared to seasonal rms differences between JPL and ECCO estimates in Figure 12a in regions associated with strong mean currents and eddies (e.g., along the Gulf Stream, Kuroshio Extension, Agulhas and Antarctic Circumpolar Currents). In particular, enhanced rms JPL and ECCO differences near the Agulhas Retroflection and the Argentine Basin could be at least partly associated with the marked seasonal intrinsic variability in the same regions (Figure 12). The expected random character of intrinsic contributions can also play a part in some of the higher phase variability in the GRACE fields compared to ECCO in regions of the Southern Ocean and the North Atlantic (cf. Figure 5). As with GAL effects, these results are only suggestive, since the ECCO optimization may fit some of the intrinsic variability present in the GRACE, thus reducing its impact on the differences in Figure 8. In addition, independent estimates of seasonal intrinsic variability in Figure 12 are needed to confirm the original results of Zhao et al. (2021).

6 Summary and Final Remarks

The available record of surface mass changes provided by GRACE and its follow-on mission is now sufficiently long to yield relatively stable estimates of the mean seasonal cycle in p_b over the global ocean, despite large variability of this seasonal cycle from year to year. Such estimates confirm the major influence of bottom topography on the amplitudes of the p_b seasonal cycle, with largest values appearing in many shallow coastal regions. There

is also enhanced variability in some deep basins (e.g., sub-polar North Pacific, Australian-Antarctic Basin) because of weakened gradients in ambient potential vorticity associated with peculiar topography and/or stronger wind forcing (e.g., Gill & Niller, 1973; Ponte, 1999; Vinogradov et al., 2008; Chen et al., 2023). Contributions from the annual term are generally the strongest, but the semi-annual harmonic is also important in several regions.

Our joint analyses of two GRACE products and a recent ECCO solution reveal good qualitative agreement among the respective mean seasonal cycle estimates, but more quantitative analysis of their differences (Figures 8 and 9) sheds light on potentially remaining deficiencies in both the gravimetry data and ECCO. In particular, differences between the JPL and GSFC GRACE products are consistent with larger data uncertainties near many coastal regions, including places where leakage of land mass signals are a well-known issue. In turn, for the ECCO estimates, the absence of GAL effects can also contribute to errors that are largest around landmasses with a strong interior mass change signal (e.g., South America, Greenland, and Gulf of Alaska). Moreover, intrinsic ocean variability, also missing in the ECCO estimates, can affect the fidelity of p_b estimates in regions of strong mean currents and eddies.

As evident from the influence of leakage of land signals onto p_b estimates, resolution is one critical element in the quest to achieve improved estimates of p_b variability and specifically its seasonal cycle. Resolution is especially important in regions with strong spatial gradients in p_b variability, like those seen in many coastal regions and adjacent continental slopes marking the transitions from the deep ocean to shallow shelves. Although the $1^\circ \times 1^\circ$ GSFC and ECCO fields can give a more refined picture of coastal p_b changes than the $3^\circ \times 3^\circ$ fields analyzed here, still finer grids will be needed to examine short scale structures of the p_b seasonal cycle in the coastal zones (e.g., Piecuch et al., 2018). Higher resolution in model-based estimates like those produced by ECCO would also allow for better representation of bottom topography and coastal dynamics.

Notwithstanding issues of spatial resolution and missing physics, the general consistency between the satellite and ECCO mean seasonal cycle estimates suggests that model-based p_b fields can be use to explore shorter spatial scales and extended periods than those allowed by the available space gravity data. In the meantime, improved sampling and other advancements, in part related to oceanographic applications, are expected from future gravity missions (Daras et al., 2024). Amid these developments, the mean seasonal cycle, given its relatively large amplitude and robust sampling statistics, remains a key metric to assess the quality of—and guide improvements to—p_b estimates from observations, models, or syntheses thereof.

Appendix A Gravitational attraction and loading

Changes in the mass distribution in any component of the Earth system affect ocean bottom pressure via the physics of gravitational attraction and loading (GAL, Vinogradova et al., 2011). Processes summarized under GAL—or self-attraction and loading in most previous works (e.g., Tamisiea et al., 2010; Vinogradova et al., 2010)—are the gravitational attraction of water toward the mass anomalies, crustal deformation under these loads, and the associated changes in Earth's gravitational field. Such gravity field perturbations act as a body force on the oceans, leading to adjustments in p_b, which we refer to as p_{GAL} hereafter. Under the assumption that the ocean's response is static (i.e., the applied loading is balanced by the resulting bottom pressure gradients), the GAL effects on p_b or sea level are commonly calculated from given surface loads by solving the sea level equation (Farrell & Clark, 1976; Tamisiea et al., 2010). Iterations are invoked to ensure the the total inferred ocean load balances the total of the loads applied. On the solution level, values of p_{GAL} can be split into

$$p_{GAL} = \frac{1}{A} \int_A p_{GAL} \mathrm{d}A + \Delta p_{GAL} \tag{A1}$$

that is, a spatial mean GAL effect, taken over the ocean with surface area A, and deviations from that mean, Δp_{GAL} (Vinogradova et al., 2010, 2011). In our analysis of the seasonal cycle, we focus on the spatially non-uniform components of p_b and hence only values of Δp_{GAL} are required. To this end, we resort to an approximation and replace the sea level equation with a much simpler, non-iterative GAL scheme adopted from tidal literature (Schindelegger et al., 2018). Suppose that a field of surface loads p' (pressure in units of equivalent water thickness) is expanded into spherical harmonics and that only elastic components participate in the GAL response. For a given degree n and order m, we then evaluate (e.g., Hendershott, 1972)

$$p^*_{GAL,nm} = \frac{3\rho_w\,(1 + k'_n - h'_n)}{\rho_e\,(2n+1)}\,p'_{nm} \tag{A2}$$

where ρ_w and ρ_e are mean densities of seawater (1030 kg m^{-3}) and the Earth (5517 kg m^{-3}), and (k'_n, h'_n) are the degree-dependent load Love numbers (H. Wang et al., 2012) in the center of figure frame. The asterisk in Eq. (A2) indicates that the quantity p^*_{GAL} synthesized from all spherical harmonic coefficients has, in general, a non-zero spatial mean. Thus, our estimate for Δp_{GAL} is

$$\Delta p_{GAL} = p^*_{GAL} - \frac{1}{A}\int_A p^*_{GAL}\,\mathrm{d}A \tag{A3}$$

We apply Eqs. (A2) and (A3) separately to the in-phase and quadrature components of the respective harmonic (either Sa or Ssa). The considered loads p' are (1) changes in land ice and terrestrial water storage, and (2) atmospheric mass variations as represented by ERA5 (Hersbach et al., 2020, 2023) surface pressures over land. For (1), we directly use Sa and Ssa estimates fitted to GRACE GSFC land values on a $1/2^\circ \times 1/2^\circ$ latitude-longitude grid. The GSFC fields are relatively smooth in space and therefore better suited than the JPL mascons for calculations involving spherical harmonics. All input fields are for the 2002–2022 time period and the spectral truncation is at $n = 179$. Note that we disregard effects of dynamic bottom pressure (Vinogradova et al., 2011), as the relevant oceanic mass loads are not easily separated from land-induced Δp_{GAL} signals in the GRACE fields and ECCO itself likely contains some oceanic GAL components (introduced by fitting to GRACE, see the main text).

Given that Eq. (A2) is central to the sea level equation calculus (see Tamisiea et al., 2010), our estimates for GAL-induced p_b fluctuations at the annual time scale are fairly consistent with Vinogradova et al. (2011)—compare their Figure 2 with Figure 10. The apparent differences are likely due to a mixture of various effects, including (i) omission of the degree-2 rotational feedback in the above procedure, (ii) differences in the temporal and spatial coverage of the input fields, (iii) finer spatial detail allowed for by our $1/2^\circ \times 1/2^\circ$ computational grid, especially near coastlines, and (iv) use of GRACE-based loads instead of numerical model results with limited fidelity over ice sheets (cf. Figure 1 in Tamisiea et al., 2010).

Appendix B Open Research

The datasets used in this study are available from the following links: JPL monthly mass grids (`https://podaac.jpl.nasa.gov/dataset/TELLUS_GRAC-GRFO_MASCON_CRI_GRID_RL06.1_V3`), GSFC global mascon solutions (`https://earth.gsfc.nasa.gov/geo/data/grace-mascons`), and ERA5 surface pressure (`https://doi.org/10.24381/cds.adbb2d47`). The p_b fields from ECCOv4r5 are available from the ECCO project upon request (`https://www.ecco-group.org/`). Harmonics shown in Figures 1–3, Matlab scripts for their calculation, and GAL data as shown in Figure 10 are provided in Zhao et al. (2024).

Acknowledgments

This work was supported by grants OCE-2239805 (NSF Physical Oceanography Program) and 80NSSC20K0728 (NASA GRACE Follow-On Science Team) to AER. M.S. acknowledges funding by the German Research Foundation (DFG, project no. 388296632). Early access to the ECCOv4r5 fields was facilitated by Ou Wang. We would like to acknowledge high-performance computing support from Cheyenne (doi:10.5065/D6RX99HX) provided by NCAR's Computational and Information Systems Laboratory, sponsored by the National Science Foundation.

References

Bingham, R. J., & Hughes, C. W. (2006). Observing seasonal bottom pressure variability in the North Pacific with GRACE. *Geophysical Research Letters*, *33*(8). Retrieved from https://agupubs.onlinelibrary.wiley.com/doi/abs/10.1029/2005GL025489 doi: https://doi.org/10.1029/2005GL025489

Chen, L., Yang, J., & Wu, L. (2023). Topography effects on the seasonal variability of ocean bottom pressure in the North Pacific Ocean. *Journal of Physical Oceanography*, *53*(3), 929–941. Retrieved from https://journals.ametsoc.org/view/journals/phoc/53/3/JPO-D-22-0140.1.xml doi: https://doi.org/10.1175/JPO-D-22-0140.1

Cheng, X., Ou, N., Chen, J., & Huang, R. X. (2021). On the seasonal variations of ocean bottom pressure in the world oceans. *Geoscience Letters*, *8*(1), 29. Retrieved from https://doi.org/10.1186/s40562-021-00199-3 doi: 10.1186/s40562-021-00199-3

Daras, I., March, G., Pail, R., Hughes, C. W., Braitenberg, C., Güntner, A., ... Pastorutti, A. (2024). Mass-change And Geosciences International Constellation (MAGIC) expected impact on science and applications. *Geophysical Journal International*, *236*(3), 1288–1308. Retrieved from https://doi.org/10.1093/gji/ggad472 doi: 10.1093/gji/ggad472

Doodson, A. T. (1928). VI. The analysis of tidal observations. *Philosophical Transactions of the Royal Society of London. Series A, Containing Papers of a Mathematical or Physical Character*, *227*, 223–279. doi: 10.1098/rsta.1928.0006

Farrell, W. E., & Clark, J. A. (1976). On postglacial sea level. *Geophysical Journal of the Royal Astronomical Society*, *46*(3), 647–667. doi: https://doi.org/10.1111/j.1365-246X.1976.tb01252.x

Forget, G., Campin, J.-M., Heimbach, P., Hill, C. N., Ponte, R. M., & Wunsch, C. (2015). ECCO version 4: an integrated framework for non-linear inverse modeling and global ocean state estimation. *Geoscientific Model Development*, *8*(10), 3071–3104. Retrieved from https://gmd.copernicus.org/articles/8/3071/2015/ doi: 10.5194/gmd-8-3071-2015

Fukumori, I., Wang, O., Fenty, I., Forget, G., Heimbach, P., & Ponte, R. M. (2019). ECCO version 4 release 4. *Tech. Rep.*. Retrieved from https://zenodo.org/record/3765929\#.X2uAv1l7l0t doi: 10.5281/zenodo.3765929

Gill, A., & Niller, P. (1973). The theory of the seasonal variability in the ocean. *Deep Sea Research and Oceanographic Abstracts*, *20*(2), 141–177. Retrieved from https://www.sciencedirect.com/science/article/pii/0011747173900491 doi: https://doi.org/10.1016/0011-7471(73)90049-1

Han, S.-C., Riva, R., Sauber, J., & Okal, E. (2013). Source parameter inversion for recent great earthquakes from a decade-long observation of global gravity fields. *Journal of Geophysical Research: Solid Earth*, *118*, 1240–1267. doi: https://doi.org/10.1002/jgrb.50116

Hendershott, M. C. (1972). The effects of solid Earth deformation on global ocean tides. *Geophysical Journal International*, *29*(4), 389–402. doi: 10.1111/j.1365-246X.1972.tb06167.x

Hersbach, H., Bell, B., Berrisford, P., Hirahara, S., Horanyi, A., et al. (2020). The ERA5 global reanalysis. *Quarterly Journal of the Royal Meteorological Society*, *146*, 1999–2049. doi: https://doi.org/10.1002/qj.3803

Hersbach, H., Bell, B., Berrisford, P., Hirahara, S., Horanyi, A., et al. (2023). *ERA5 hourly*

data on single levels from 1940 to present. Copernicus Climate Change Service (C3S) Climate Data Store (CDS). doi: 10.24381/cds.adbb2d47

Hughes, C. W., Williams, J., Blaker, A., Coward, A., & Stepanov, V. (2018). A window on the deep ocean: The special value of ocean bottom pressure for monitoring the large-scale, deep-ocean circulation. *Progress in Oceanography*, *161*, 19–46. doi: https://doi.org/10.1016/j.pocean.2018.01.011

Johnson, G. C., & Chambers, D. P. (2013). Ocean bottom pressure seasonal cycles and decadal trends from GRACE Release-05: Ocean circulation implications. *Journal of Geophysical Research: Oceans*, *118*(9), 4228–4240. Retrieved from https://agupubs.onlinelibrary.wiley.com/doi/abs/10.1002/jgrc.20307 doi: https://doi.org/10.1002/jgrc.20307

Kanzow, T., Flechtner, F., Chave, A., Schmidt, R., Schwintzer, P., & Send, U. (2005). Seasonal variation of ocean bottom pressure derived from Gravity Recovery and Climate Experiment (GRACE): Local validation and global patterns. *Journal of Geophysical Research: Oceans*, *110*(C9). Retrieved from https://agupubs.onlinelibrary.wiley.com/doi/abs/10.1029/2004JC002772 doi: https://doi.org/10.1029/2004JC002772

Landerer, F. W., Flechtner, F. M., Save, H., Webb, F. H., Bandikova, T., Bertiger, W. I., ... Yuan, D.-N. (2020). Extending the global mass change data record: GRACE Follow-On instrument and science data performance. *Geophysical Research Letters*, *47*(12), e2020GL088306. Retrieved from https://agupubs.onlinelibrary.wiley.com/doi/abs/10.1029/2020GL088306 (e2020GL088306 2020GL088306) doi: https://doi.org/10.1029/2020GL088306

Loomis, B. D., Luthcke, S. B., & Sabaka, T. J. (2019). Regularization and error characterization of GRACE mascons. *Journal of Geodesy*, *93*, 1381–1398. doi: https://doi.org/10.1007/s00190-019-01252-y

Peralta-Ferriz, C., & Morison, J. (2010). Understanding the annual cycle of the Arctic Ocean bottom pressure. *Geophysical Research Letters*, *37*(10). Retrieved from https://agupubs.onlinelibrary.wiley.com/doi/abs/10.1029/2010GL042827 doi: https://doi.org/10.1029/2010GL042827

Piecuch, C. G. (2015). Bottom-pressure signature of annual baroclinic Rossby waves in the northeast tropical Pacific Ocean. *Journal of Geophysical Research: Oceans*, *120*(4), 2449–2459. Retrieved from https://agupubs.onlinelibrary.wiley.com/doi/abs/10.1002/2014JC010667 doi: https://doi.org/10.1002/2014JC010667

Piecuch, C. G., Fukumori, I., Ponte, R. M., Schindelegger, M., Wang, O., & Zhao, M. (2022). Low-frequency dynamic ocean response to barometric-pressure loading. *Journal of Physical Oceanography*, *52*(11), 2627–2641. Retrieved from https://journals.ametsoc.org/view/journals/phoc/52/11/JPO-D-22-0090.1.xml doi: 10.1175/JPO-D-22-0090.1

Piecuch, C. G., Landerer, F. W., & Ponte, R. M. (2018, 05). Tide gauge records reveal improved processing of gravity recovery and climate experiment time-variable mass solutions over the coastal ocean. *Geophysical Journal International*, *214*(2), 1401-1412. Retrieved from https://doi.org/10.1093/gji/ggy207 doi: 10.1093/gji/ggy207

Piecuch, C. G., & Ponte, R. M. (2014). Annual Cycle in Southern Tropical Indian Ocean Bottom Pressure. *Journal of Physical Oceanography*, *44*(6), 1605–1613. Retrieved from https://journals.ametsoc.org/view/journals/phoc/44/6/jpo-d-13-0277.1.xml doi: https://doi.org/10.1175/JPO-D-13-0277.1

Ponte, R. M. (1999). A preliminary model study of the large-scale seasonal cycle in bottom pressure over the global ocean. *Journal of Geophysical Research: Oceans*, *104*(C1), 1289–1300. Retrieved from https://agupubs.onlinelibrary.wiley.com/doi/abs/10.1029/1998JC900028 doi: https://doi.org/10.1029/1998JC900028

Ponte, R. M., Quinn, K. J., Wunsch, C., & Heimbach, P. (2007). A comparison of model and GRACE estimates of the large-scale seasonal cycle in ocean bottom pressure. *Geophysical Research Letters*, *34*(9). Retrieved from https://agupubs.onlinelibrary

.wiley.com/doi/abs/10.1029/2007GL029599 doi: https://doi.org/10.1029/2007GL029599

Ray, R. D., Loomis, B. D., & Zlotnicki, V. (2021). The mean seasonal cycle in relative sea level from satellite altimetry and gravimetry. *Journal of Geodesy*, *95*(7), 80. Retrieved from https://doi.org/10.1007/s00190-021-01529-1 doi: 10.1007/s00190-021-01529-1

Schindelegger, M., Green, J. A. M., Wilmes, S.-B., & Haigh, I. D. (2018). Can we model the effect of observed sea level rise on tides? *Journal of Geophysical Research: Oceans*, *123*(7), 4593–4609. doi: 10.1029/2018JC013959

Tamisiea, M. E., Hill, E. M., Ponte, R. M., Davis, J. L., Velicogna, I., & Vinogradova, N. T. (2010). Impact of self-attraction and loading on the annual cycle in sea level. *Journal of Geophysical Research: Oceans*, *115*(C7). doi: https://doi.org/10.1029/2009JC005687

Tapley, B. D., Bettadpur, S., Watkins, M., & Reigber, C. (2004). The gravity recovery and climate experiment: Mission overview and early results. *Geophysical Research Letters*, *31*(9). Retrieved from https://agupubs.onlinelibrary.wiley.com/doi/abs/10.1029/2004GL019920 doi: https://doi.org/10.1029/2004GL019920

Vinogradov, S. V., Ponte, R. M., Heimbach, P., & Wunsch, C. (2008). The mean seasonal cycle in sea level estimated from a data-constrained general circulation model. *Journal of Geophysical Research: Oceans*, *113*(C3). Retrieved from https://agupubs.onlinelibrary.wiley.com/doi/abs/10.1029/2007JC004496 doi: https://doi.org/10.1029/2007JC004496

Vinogradova, N. T., Ponte, R. M., Tamisiea, M. E., Davis, J. L., & Hill, E. M. (2010). Effects of self-attraction and loading on annual variations of ocean bottom pressure. *Journal of Geophysical Research: Oceans*, *115*(C6). Retrieved from https://agupubs.onlinelibrary.wiley.com/doi/abs/10.1029/2009JC005783 doi: https://doi.org/10.1029/2009JC005783

Vinogradova, N. T., Ponte, R. M., Tamisiea, M. E., Quinn, K. J., Hill, E. M., & Davis, J. L. (2011). Self-attraction and loading effects on ocean mass redistribution at monthly and longer time scales. *Journal of Geophysical Research: Oceans*, *116*(C8). doi: https://doi.org/10.1029/2011JC007037

Wang, H., Xiang, L., Jia, L., Jiang, L., Wang, Z., Hu, B., & Gao, P. (2012). Load Love numbers and Green's functions for elastic Earth models PREM, iasp91, ak135, and modified models with refined crustal structure from Crust 2.0. *Computers & Geosciences*, *49*, 190–199. doi: https://doi.org/10.1016/j.cageo.2012.06.022

Wang, O., Fukumori, I., & Fenty, I. (2020). ECCO version 4 release 4 user guide. *JPL Doc.*. Retrieved from https://ecco-group.org/docs/v4r4_user_guide.pdf

Watkins, M. M., Wiese, D. N., Yuan, D.-N., Boening, C., & Landerer, F. W. (2015). Improved methods for observing Earth's time variable mass distribution with GRACE using spherical cap mascons: Improved Gravity Observations from GRACE. *J. Geophys. Res.: Solid Earth*, *120*(4), 2648–2671. doi: 10.1002/2014JB011547

Wiese, D. N., Landerer, F. W., & Watkins, M. M. (2016). Quantifying and reducing leakage errors in the JPL RL05M GRACE mascon solution. *Water Resources Research*, *52*(9), 7490–7502. Retrieved from https://agupubs.onlinelibrary.wiley.com/doi/abs/10.1002/2016WR019344 doi: https://doi.org/10.1002/2016WR019344

Wiese, D. N., Yuan, D.-N., Boening, C., Landerer, F. W., & Watkins, M. M. (2023). *JPL GRACE and GRACE-FO Mascon Ocean, Ice, and Hydrology Equivalent Water Height Coastal Resolution Improvement (CRI) Filtered Release 06.1 Version 03.* NASA Physical Oceanography Distributed Active Archive Center. Retrieved from https://podaac.jpl.nasa.gov/dataset/TELLUS_GRAC-GRFO_MASCON_CRI_GRID_RL06.1_V3 doi: 10.5067/TEMSC-3JC63

Wunsch, C. (1996). Frontmatter. In *The ocean circulation inverse problem* (p. i-vi). Cambridge University Press.

Wunsch, C., Heimbach, P., Ponte, R. M., Fukumori, I., & Members, T. E.-G. C. (2009, June). The global general circulation of the ocean estimated by the ECCO-consortium. *Oceanography*, *22(2)*. Retrieved from https://doi.org/10.5670/oceanog.2009.41

Xiong, X., Cheng, X., Ou, N., Feng, T., Qin, J., Chen, X., & Huang, R. X. (2022). Dynamics of seasonal and interannual variability of the ocean bottom pressure in the Southern Ocean. *Acta Oceanologica Sinica*, *41*(5), 78–89. Retrieved from https://doi.org/10.1007/s13131-021-1878-z doi: 10.1007/s13131-021-1878-z

Zhao, M., Ponte, R. M., Penduff, T., Close, S., Llovel, W., & Molines, J.-M. (2021). Imprints of ocean chaotic intrinsic variability on bottom pressure and implications for data and model analyses. *Geophysical Research Letters*, *48*(24), e2021GL096341. Retrieved from https://agupubs.onlinelibrary.wiley.com/doi/abs/10.1029/2021GL096341 (e2021GL096341 2021GL096341) doi: https://doi.org/10.1029/2021GL096341

Zhao, M., Schindelegger, M., & Ponte, R. (2024). *How well do we know the seasonal cycle in ocean bottom pressure?* Zenodo. Retrieved from https://doi.org/10.5281/zenodo.10685748 doi: 10.5281/zenodo.10685748

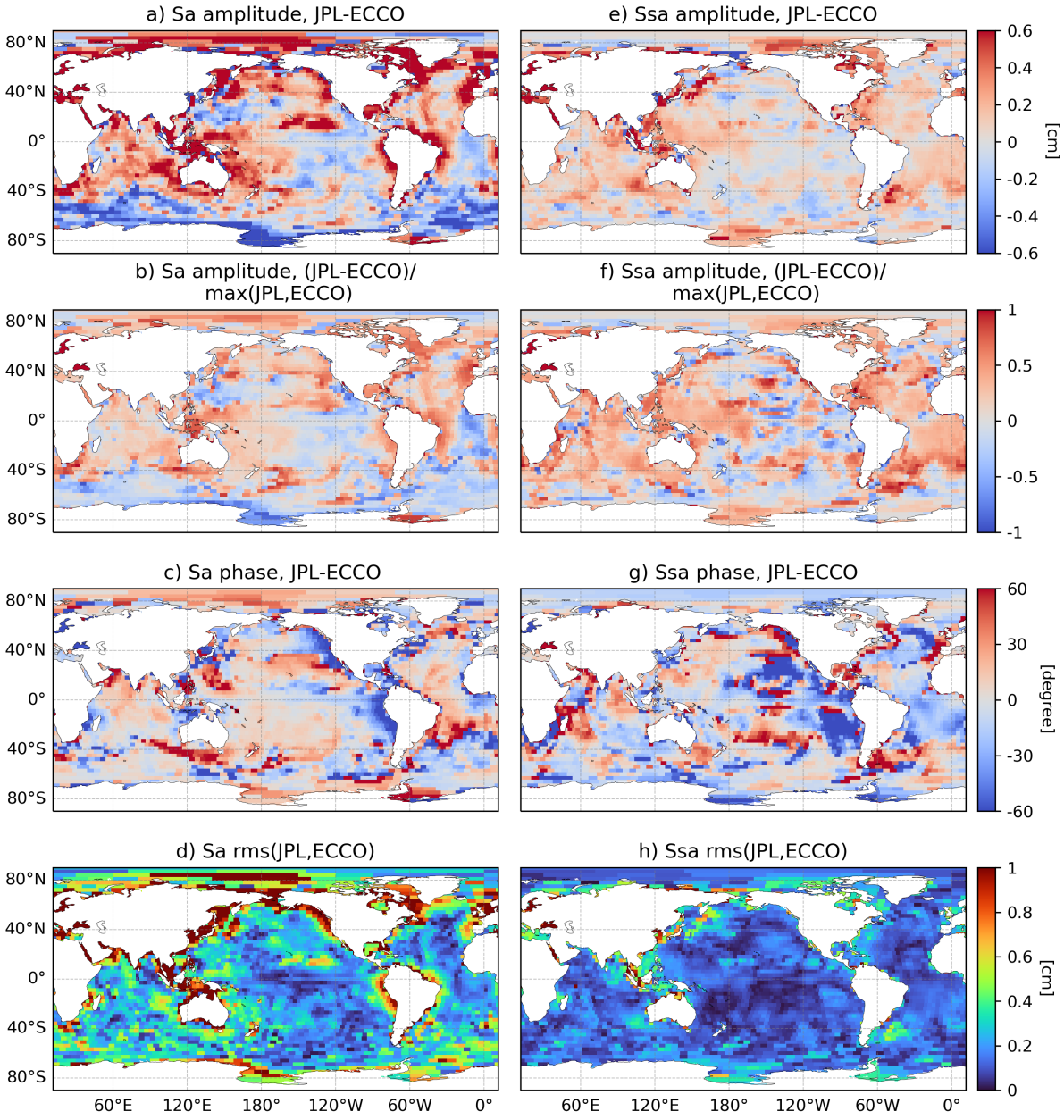

Figure 8. Assessment of differences between JPL GRACE and ECCO for annual (left) and semiannual (right) harmonics: (a,e) JPL minus ECCO amplitudes; (b,f) Magnitude of the ratio of JPL minus ECCO amplitude to max(JPL, ECCO) amplitude; (c,g) JPL minus ECCO phases; (d,h) Root-mean-square difference between JPL and ECCO.

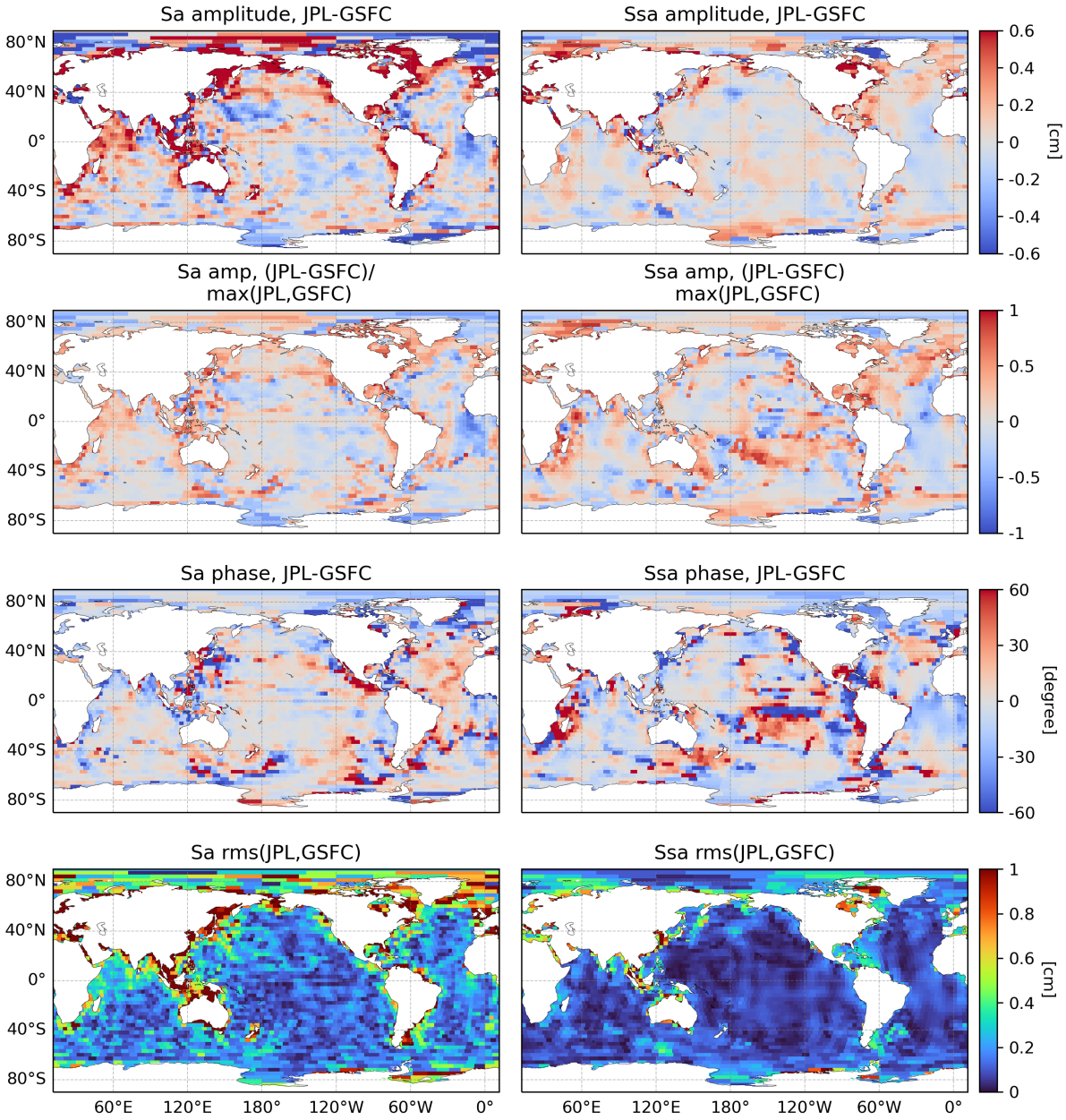

Figure 9. As in Figure 8 but for the differences between JPL and GSFC mascons.

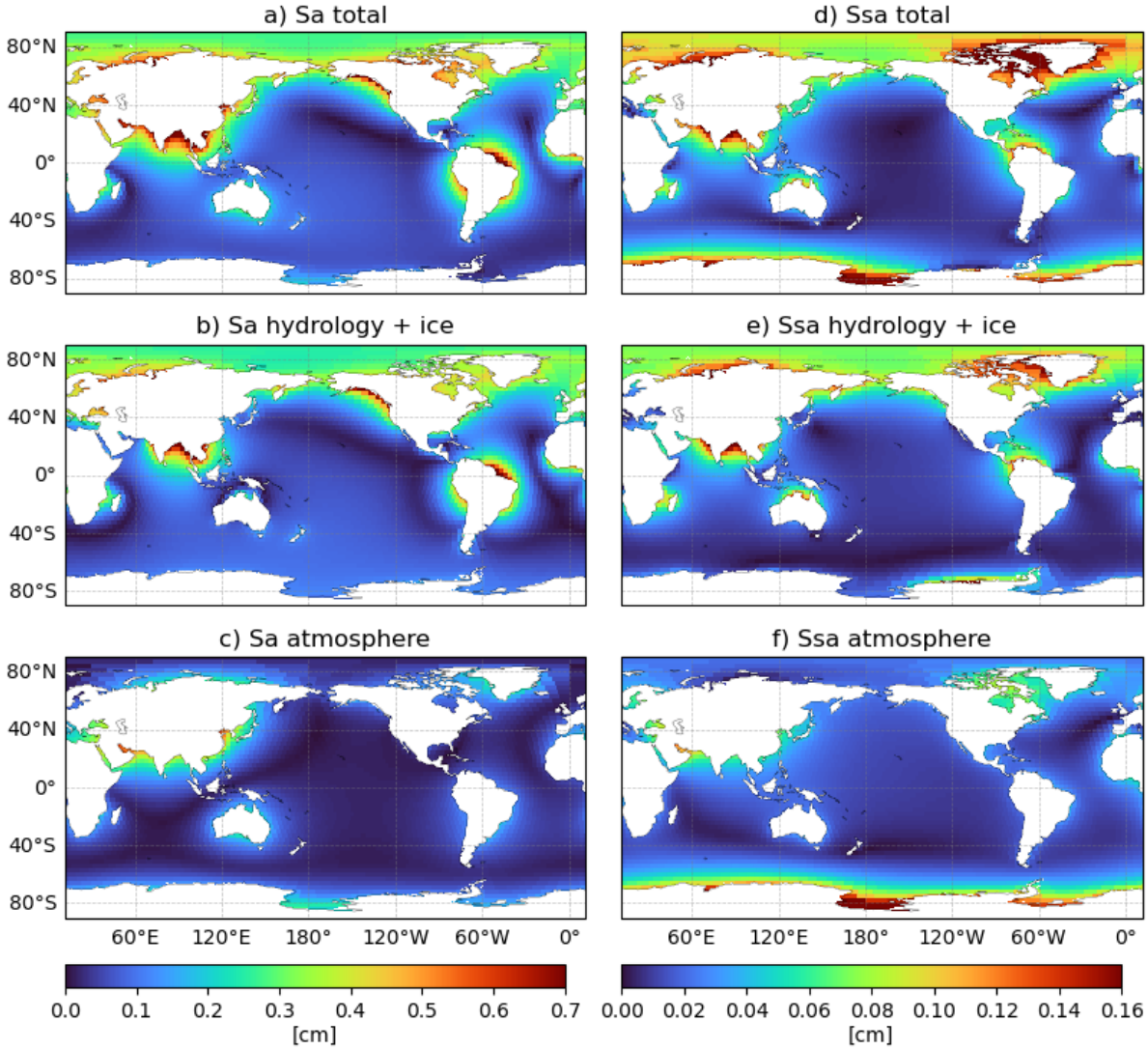

Figure 10. Standard deviation of Sa (left) and Ssa (right) harmonics for gravitational attraction and loading (GAL) effects on ocean mass redistribution due to seasonal changes in land ice, terrestrial water storage, and atmospheric mass over land. Panels (a,d) show the net GAL effect of these loads, made up by contributions from ice and hydrology (b,e) and the atmosphere (c,f).

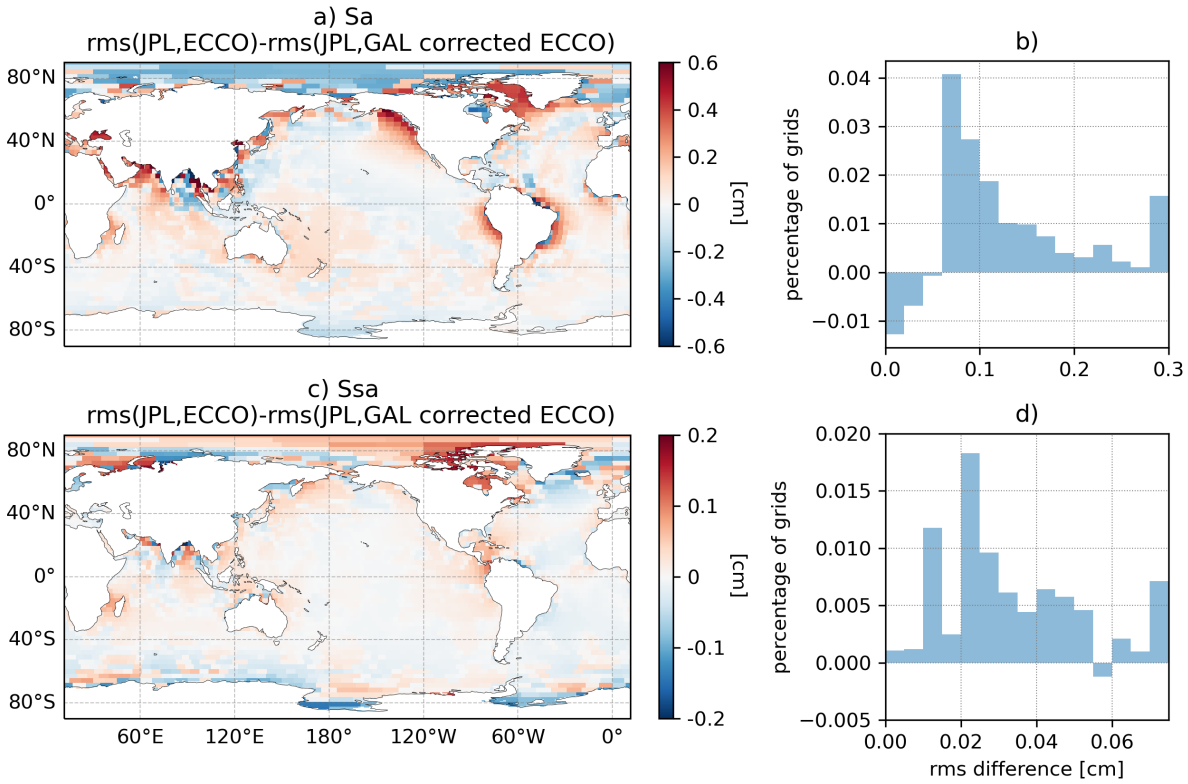

Figure 11. Root-mean-square difference between JPL and ECCO estimates minus rms difference between JPL and ECCO plus GAL fields, for Sa (a) and Ssa (c). Difference between positive and negative values of area-weighted histograms are shown to the right (b,d). The bar at the endpoint represents the cumulative tail values. Positive values cover $\sim 56\%$ (Sa) and 55% (Ssa) of the global ocean area.

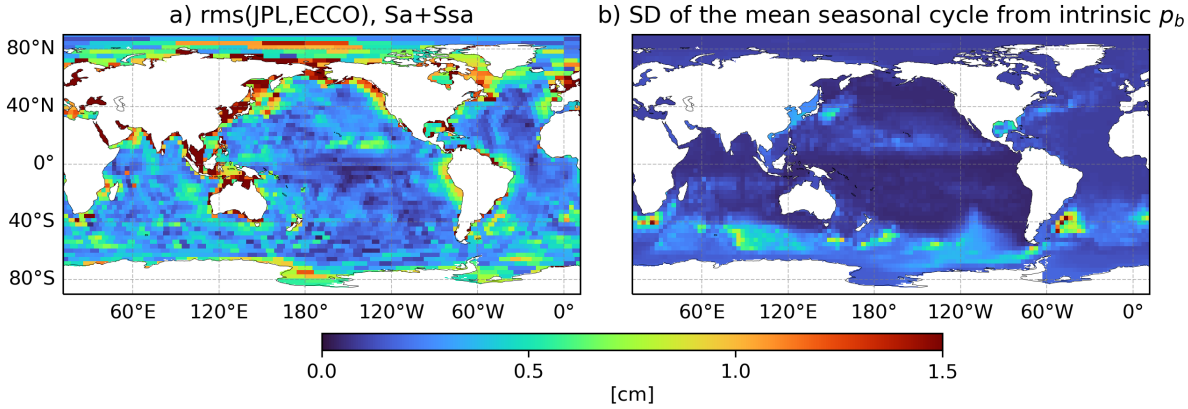

Figure 12. (a) Root-mean-square difference between JPL and ECCO estimates for the combined Sa and Ssa harmonics. (b) Standard deviation in cm of the mean seasonal cycle in p_b associated with intrinsic ocean variability, reproduced from Figure 3 of Zhao et al. (2021). Here, the mean seasonal cycle is defined based on monthly mean composites; see Zhao et al. (2021) for details.